communications chemistry

Article

https://doi.org/10.1038/s42004-024-01353-6

Chromatin inspired bio-condensation between biomass DNA and guanosine monophosphate produces all-nucleic hydrogel as a hydrotropic drug carrier

Check for updates

Suryakamal Sarma[1], Neha Thakur[2], Nidhi Varshney[3], Hem Chandra Jha[3] & Tridib K. Sarma[1]

The integration of biomolecules into supramolecular nanostructures forms the basis of the natural world. Naturally occurring liquid-liquid phase separation resulting in biomolecular condensates has inspired the formation of biomolecule-based smart materials with multi-dimensional applications. A non-covalent bio-condensation between biomass DNA and guanosine monophosphate (GMP) has been described, mimicking chromatin folding and creating a unique "all-nucleic" DNA-GMP condensates. These condensates initiate the formation of G-quadruplex-based superstructures, assembling into super-helical fibres driven by synergistic hydrogen bonding and stacking, which have been thoroughly investigated. This simple, one-step method for the bio-condensation of biomass DNA leads to an "all-nucleic" hydrogel with higher-order self-assembly and excellent mechanical properties. While most of the reported DNA based biomaterials, including hydrogels, require precisely sequenced and molecularly architectured DNA building blocks, we have developed a simple, universal, and facile bio-condensation method that utilizes biomass DNA acquired from any bio-resource to fabricate DNA hydrogels. The hydrogel efficiently encapsulates and sustains the release of both hydrophilic and hydrophobic drugs, demonstrating its competency as a drug carrier. We believe this energy-efficient and low-cost method represents a new technique for using biomass DNA as building blocks for the next generation of soft materials.

Within cells, subcellular controlled microenvironments or compartments have evolved to facilitate and regulate specific biocatalytic processes, with some characterized by membrane-bound structures composed of lipid bilayers, while others exist in a membrane-less form resulting from the phase separation of proteins and nucleic acids[1,2]. Liquid–liquid phase transition of biological macromolecules result in the formation of the non-membrane-bound compartments such as the nucleoli, centrosomes, stress granules etc[3–5]. For example, in eucaryotic cells, genomic DNA packaged into chromatin, primarily guided by the core histone and linker histone proteins, forming an octamer of histones, which eventually forms left-handed hierarchical superhelix[6,7]. These chromatin structures essentially control all nuclear processes involving DNA, including transcription, DNA replication, and DNA repair[8,9]. These natural compartments have inspired the creation of synthetic microenvironments or bio condensates for purposes like accelerating enzymatic reactions, aiding small molecule synthesis, and delivering drugs or therapeutic biomolecules[10,11]. Liquid phase condensation of DNA resulting in the formation of biomolecular condensates such as concentrated droplets, gels, or reversible aggregates via associative interactions have inspired material scientists for fabrication of various functional materials[12,13]. DNA is a versatile and abundant biomass (estimated at 50 billion metric tons)[14,15] and can be used to form a variety of novel biohybrid materials such as DNA gels[16,17], DNA dendrimers[18], DNA nanoflowers[19], three-dimensional crystals[20,21], DNA origami[22], constitutional dynamic networks[23] etc.

Most of the biological phase separations of DNA involve polyelectrolytes with nonuniform charge distribution and multivalent reciprocity associated via electrostatic interactions. However, the bio-condensation of DNA via non-electrostatic association that involves the formation of such as

[1]Department of Chemistry, Indian Institute of Technology Indore, Indore, India. [2]Developmental Bioengineering, TechMed Centre, University of Twente. Drienerlolaan 5, Enschede, The Netherlands. [3]Department of Biosciences and Biomedical Engineering, Indian Institute of Technology Indore, Indore, India. e-mail: tridib@iiti.ac.in

G-quadruplexes (G4), has been less exploited. G4s play an important role in several cellular pathways that include DNA replication, gene expression and telomere maintenance[24]. Herein, we describe a non-covalent bio-condensation between DNA and guanosine monophosphate (GMP) that mimics chromatin folding, resulting in unique "all-nucleic" DNA-GMP condensates. This synergy leads to the formation of G4-based superstructures, which ultimately assemble into super-helical fibers. The unique hierarchical self-assembly of randomly coiled DNA into an ordered fibrillar network, the evolution of helicity in these fibers, and the extent of condensation through synergistic hydrogen bonding and stacking have been thoroughly investigated. Additionally, the dynamic reconfigurability of these condensates through mass transition and thermodynamic aspects has also been investigated. Interestingly, this bio-condensation at higher concentration, can be extended to a supramolecular "all nucleic" hydrogel with excellent mechanical properties. The transformation of randomly coiled biomass DNA to an ordered helical G-quadruplex superstructures through non-covalent interactions induce reconfiguration and switch-ability to the hydrogel, that result in diverse applications such as stimuli responsiveness, self-healing, sustained drug release etc. Utilizing biomass DNA as a building polymeric block for smart DNA-based materials is gaining attention due to the complexity and cost associated with cascade self-assembly of carefully sequenced and patterned oligonucleotides and DNA scaffolds[25–28].

The "all nucleic" biomass DNA hydrogel reported herein has several advantages: (a) all raw materials are nucleic acids (or fragments) derived from bio-resources, (b) the method is green and spontaneous, involving no synthetic steps, thereby can be translated to industrial scale easily, (c) the resultant hydrogel is highly stable, reusable and biocompatible. Furthermore, the hydrogel can encapsulate a variety of drug molecules, both hydrophilic and hydrophobic, with a high loading capacity and shows sustained drug release. To the best of our knowledge, this is the first report of a biomass DNA hydrogel formed through physical crosslinking involving a nucleotide.

Results and discussions

Chromatin inspired "all nucleic" G4-condensation

In cells, arrays of nucleosomes organize the DNA within chromatin. Each nucleosome core comprises of an octamer assembled from two copies each of histone proteins, around which 145-147 base pairs of DNAs are wrapped. The nucleosome's histone octamer core constitutes a left-handed protein superhelix composed of four histone dimers arranged spirally[6,8]. Similar to the histones, four guanine bases can associate through Hoogsteen hydrogen bonding to form a guanine tetrad, having square planner structure. Two or more guanine tetrads stack on top of each other to form G-quadruplexes, stabilized by a cation such as K^+, Na^+, NH_4^+ *etc*[29–31]. Inspired from the DNA packaging of chromatin guided by linker and core histones, it could be expected that bio-condensation of DNA can occur through wrapping around the G4 assembly. Interestingly, we observed that DNA and GMP have synergistic effect towards the formation of the bio-condensate, where DNA facilitates the G4 formation, which in turn induce condensation of DNA leading to a helical self-assembly similar to DNA packaging around the histone proteins in chromatin (Scheme 1).

A simple mixing of salmon milt biomass DNA (40 μg/mL) and 150 μM GMP-Na_2 at 37 °C under physiological pH of 7.4 and further incubation for 12 h led to the formation of a bio-condensate. Salmon milt biomass DNA was used for the studies due to their commercial availability and low cost. The first evidence for the condensation was obtained from the Tyndall effect shown in the solution containing both DNA and GMP (Supplementary Fig. 1). Scanning electron microscope (SEM) images showed highly entangled fibrillar network with an average diameter of 240 ± 15 nm of each fiber (Fig. 1a and Supplementary Fig. 2A). The nanofibers bundled together to form larger fibers, as confirmed by the high-resolution SEM images shown in Supplementary Fig. 2B. Transmission electron microscopy (TEM) studies further confirmed the formation of highly intertwined fibrillar morphology with an average diameter of 23 ± 8 nm as calculate through mean width calculation (Supplementary Fig. 3). High-resolution TEM images showed the helical superstructure formation of the DNA-GMP condensates (Fig. 1b). Further, Atomic force microscopy studies validated the formation of fibrillar nanostructures with an average height of 12 nm (Supplementary Fig. 4).

Various spectroscopic studies were carried out to understand the supramolecular interactions leading to the bio-condensation. The absorption spectrum of GMP, having λ_{max} at 251 nm exhibit a bathochromic shift upon addition of biomass DNA, indicating the formation of a non-covalent assembly[32] (Supplementary Fig. 5). Circular dichroism spectroscopy reveals the formation of G4-condensation with a negative cotton band at 250 nm following an antiparallel G-quartet pattern[33,34] (Fig. 1c). The negative cotton band at 250 nm showed an incremental enhancement until a stoichiometry of 1:1 molar ratio of DNA and GMP, inferring the optimum formation of G-quadruplexes under these conditions (Supplementary Fig. 6). Further, Job's plot confirms that the DNA and GMP condenses at 1:1 stoichiometry in the concentration of 0.04 mg/mL DNA and 150 μM GMP (Supplementary Fig. 7). The ^{1}H-NMR spectrum of the DNA-GMP condensate shows a broad peak in the 10-12 ppm range, characteristic of G4 formation associated with the imino protons of guanine in a G-tetrad (Fig. 1d)[35,36]. Due to the presence of the DNA macromolecule, the imino proton signals of the GMP guanine moieties overlap in this region (Fig. 1e), resulting in a relatively broad and flat peak in the full NMR spectrum (Supplementary Fig. 8). While this broad peak does not confirm the exact G4 conformation, it does indicate the formation of a G4 network through the self-assembly of GMP molecules. Zeta potential measurements were also carried out to evaluate the changes in the surface charge of DNA, GMP, and the DNA-GMP condensate. The zeta potential of DNA and GMP changed from −46.36 mV and −28.39 mV, respectively to −21.18 mV upon condensate formation (Supplementary Fig. 9). The acidic nature of DNA promotes the self-assembly of GMP into G4 strands, suggesting that biomass DNA condensation is facilitated in an acidic environment, where DNA macromolecules and self-assembled GMP molecules are likely to interact through hydrogen bonding between their phosphate groups. Additionally, Na^+ ions occupy the G4 cavities, forming a positively charged ion channel after the condensation of DNA and GMP. This positive ion channel, along with the stabilization of phosphate groups through non-covalent interactions, contributes to the reduction of the overall negative surface charge of the DNA-GMP condensate.

For a deeper understanding of the condensation process, a thorough mechanistic analysis was conducted. First, circular dichroism (CD) spectroscopy was conducted to confirm the extent of formation of G4 assembly upon addition of variable amount of GMP at fixed DNA concentration as shown in Fig. 2a. The ellipticity showed a sigmoidal decrease from $\theta_{250\ nm} = -0.2$ to $\theta_{250\ nm} = -0.8$, suggesting an increase in G4 formation with an increase in GMP concentration (Fig. 2b). The possibility of DNA-wrapped π-π stacked G4 moieties leading to nano-fibrillation in the condensate were confirmed by a Thioflavin T (ThT) assay. The fluorogenic dye ThT is widely used for the detection of G4 motifs through fluorescence light-up in the visible region[37]. The non-covalent interactions between ThT and G4 channel stabilize the dye in a rigid, planar structure via end stacking, groove binding, or intercalation, thus greatly reducing its usual nonradiative torsional relaxation. This results in fluorescence enhancement by several folds[38,39]. Concomitant to the G4 formation, the fluorescence emission spectra of ThT-assay showed a remarkable linear increase in the intensity (FL/FL_0) from 22-fold (due to intrinsic affinity of ThT towards biomass DNA) to 30-fold at a GMP concentration of 150 μM ($\lambda_{em}^{max} = 491$ nm) (Fig. 2c, d). This suggests that G4 formation and stacked fibrillation can be regulated with the amount of GMP. The results suggest an interesting pathway leading to the fibrillar condensates, where DNA induces the formation of G4-moieties and subsequent π-π stacked supramolecular nanostrands. Simultaneously, DNA wraps around the G4 strands to form helical fibrils leading to the condensates, following a pathway similar to that of chromatins.

To gain more insight into the self-assembly process and the underlying interactions during the bio-condensation of DNA and GMP, concentration-

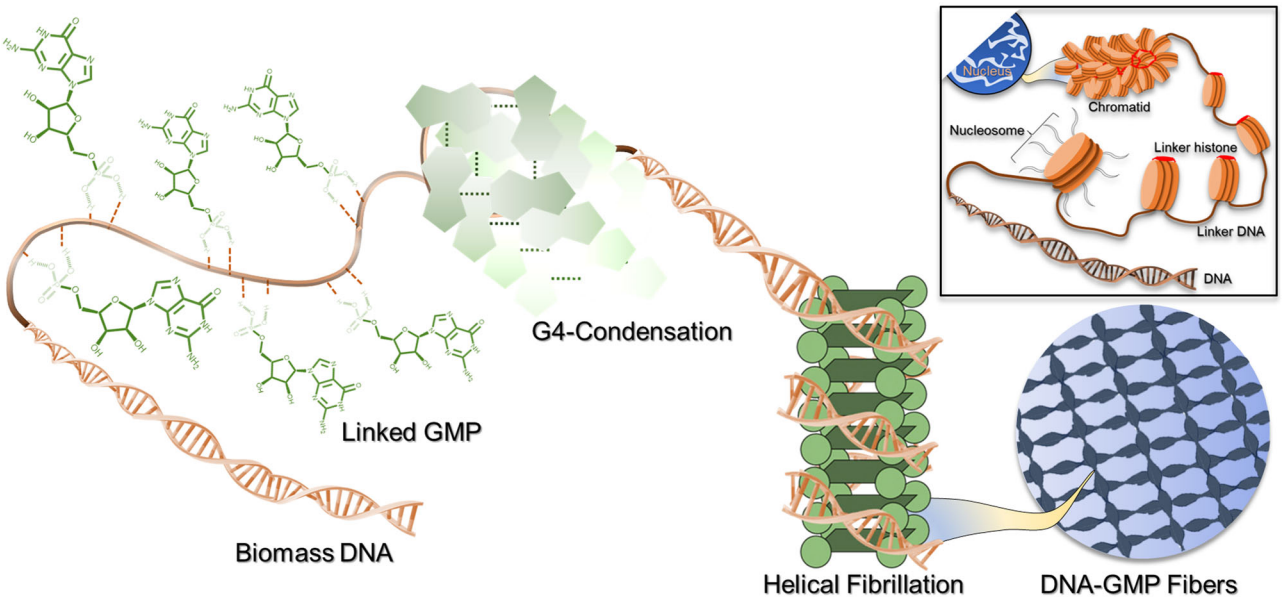

Scheme 1 | Chromatin-inspired DNA packaging into a G4-condensate leads to the formation of a helical fibril network. From left to right: the chemical structure of the guanosine monophosphate nucleotide is followed by a schematic diagram of G4-condensation and the formation of a DNA-wrapped π-π stacked helical superstructure.

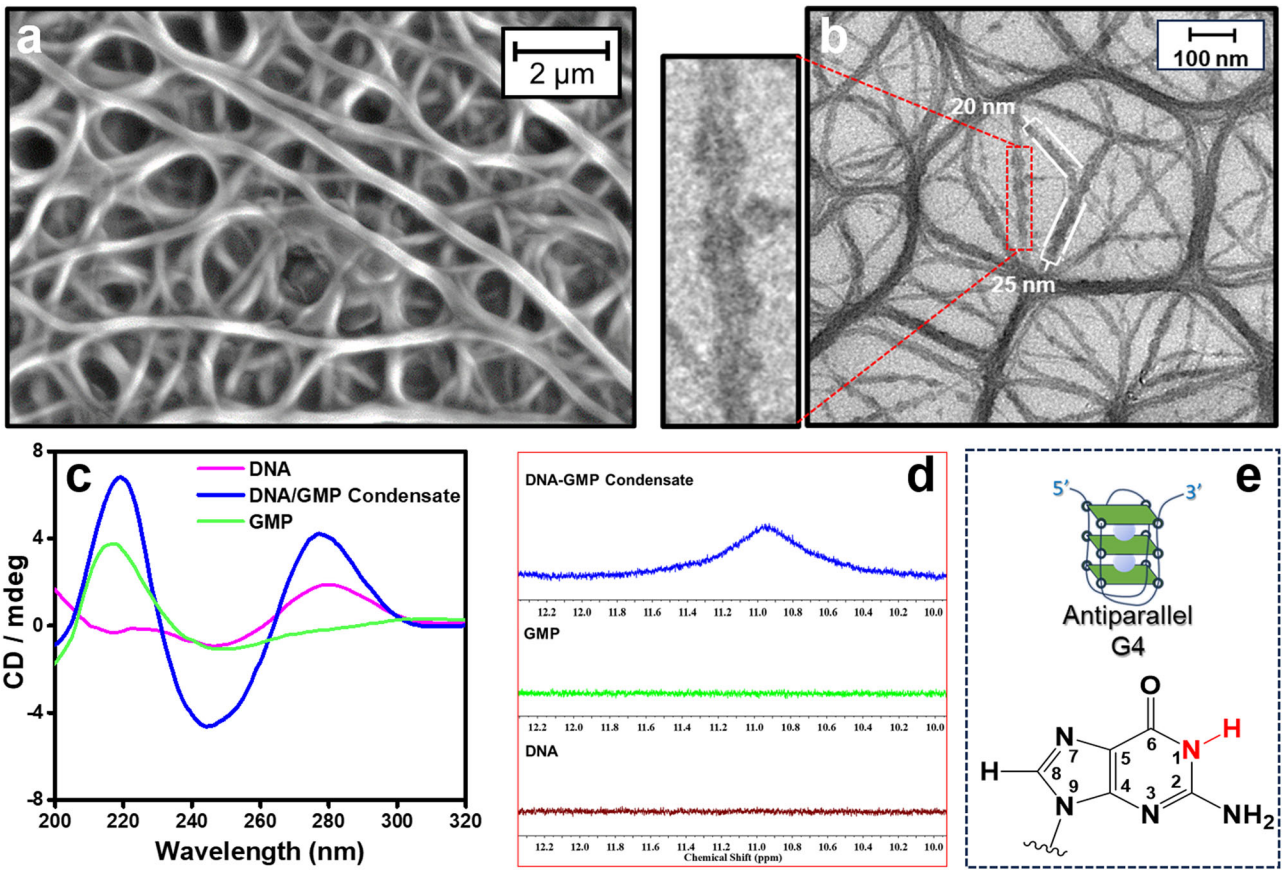

Fig. 1 | Morphological and spectroscopic evaluation of the DNA-GMP condensate. a FE-SEM image showing the entangled fibrillar network, (**b**) HRTEM image of the fibers showing the helicity (inset) of the fibers, (**c**) Circular dichroism spectrum of DNA-GMP fibers showing the formation of anti-parallel G4, (**d**) ^{1}H-NMR shift showing the formation of G4 in the region of 10-12 ppm for the imino proton (H-1 shown at inset) of guanine base and (**e**) Chemical structures illustrating the antiparallel G4 and the guanine moiety, with emphasis on the imino proton.

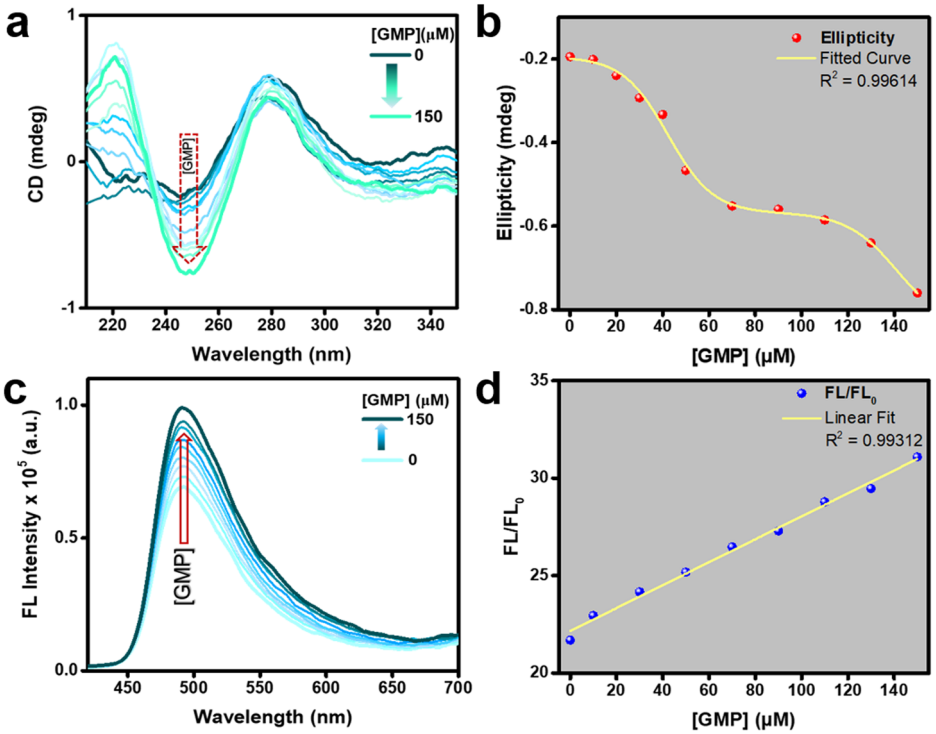

Fig. 2 | Spectroscopic investigations into the concentration-dependent dynamics of the condensation process. a CD spectra at various GMP concentration (0–150 μM) and constant DNA amount (40 μg/mL) with incremental negative cotton band at 250 nm, (**b**) sigmoidal decrease in the ellipticity at 250 nm, (**c**) FL spectra of ThT assay (ThT concentration 10 μM) at various GMP concentration from 0 to 150 μM and constant DNA concentration (40 μg/mL) and (**d**) Linear incremental fitting of FL/FL_0 ratio for ThT assay.

dependent aggregation kinetic studies were carried out using various microscopic techniques. Since GMP played a key role in the G4 assembly and stacked fibrillation, we monitored the morphological evolution at various GMP concentrations, while keeping the DNA concentration (40 μg/mL) fixed. The random DNA biopolymers started to organize into small self-assembled nanoaggregates, even when 10 μM of GMP was added, suggesting that DNA starts to organize around the G4 formed even at such a low concentration of GMP (Supplementary Fig. 10A, B). At an increased GMP concentration of 30 μM, with more G4 core formation, DNA is adsorbed onto the surface and self-assembled into a spherical hollow superstructure with a corona-like formation (Fig. 3a). Upon further enhancing the GMP concentration to 50 μM, the stacked fibrillation process starts with the appearance of anisotropic nano-blocks along with unwrapped DNAs as shown in Fig. 3b. At an increased GMP concentration of 70 μM, non-covalent interactions between G4-tetrads and DNA wrapping around the G4 strands led to the formation of elongated rod-like structures with prominent helical chirality (Supplementary Fig. 10E). The concentration-dependent anisotropic growth was further evident at a GMP concentration of 90 μM, as the nano-fibrillation took precedence (Fig. 3c), which further crosslinked to form a dense entangled fibril network at GMP concentrations of 120 and 150 μM (Fig. 3d and S10H). Thus, it can be inferred that at higher concentrations (>100 μM) of GMP, all the randomly aggregated DNA coils uniformly wrap around the G4-moieties and form π-π stacked helical DNA-GMP fibrillar condensates. Atomic force microscopy (AFM) studies of the condensates at variable concentration of GMP (at a fixed concentration of DNA) further confirmed the growth pattern from small anisotropic building blocks to the highly entangled fibrillar network with increasing concentration of GMP from 50 to 150 μM (Fig. 3e–h and Supplementary Fig. 11). Interestingly, the height profile of the nanoaggregates at lower GMP concentration (50 and 70 μM) showed much higher average height (~50 nm) as compared to the height of the nanofibrils formed (~12 nm) at higher concentration (120 and 150 μM). Probably, unwrapped DNA is adsorbed over the aggregates at lower GMP concentration, whereas DNA wraps around the G4 strands uniformly leading to the fibrillar network at higher GMP concentration.

To further understand the involvement of π-π stacking during the anisotropic morphology evolution of the DNA-GMP condensations, confocal laser microscopy studies were carried out using Thioflavin-T labeling at variable GMP concentrations, while keeping DNA concentration fixed (40 μg/mL). Thioflavin-T binds to G4 fibril channels, resulting in the fluorescence enhancement in the green region[37,38]. Figure 3i–l shows the confocal fluorescence microscopy images of the ThT-labeled DNA/GMP condensates. At a very low GMP concentration of 10 μM, only blue fluorescence was observed owing to the intrinsic fluorescence of DNA. This suggests the presence of large amount of random DNA at the initial stage of G4 formation (Fig. 3i). When the GMP concentration was increased to 50 μM, the formation of nanoaggregates could be observed in the bright field image, however these aggregates also showed blue fluorescence (Fig. 3j). As the GMP concentration increased to 90 μM, the nano-fibrillation process started, as indicated by the appearance of green fluorescence alongside the intrinsic DNA emission in the ThT assay (Fig. 3k). This co-localization of DNA nanoaggregates and the G4 fibrillar network was observed in various regions, as shown in Supplementary Fig. 12. At a higher GMP concentration (150 μM), predominant green fluorescence was observed from the homogeneous fibrillar condensate, suggesting that all DNA macromolecules participate in the condensation, resulting in strong green fluorescence from ThT bound to the π-π stacked G4 fibers (Fig. 3l). At lower concentration of GMP, due to the abundance of randomly coiled DNA, the weak blue intrinsic emission of DNA was predominant. With an increase in GMP concentration, the green emission emanating from the G4 stacking emerged, along with the blue fluorescence of DNA. At the optimum GMP concentration (150 μM), the formation of homogeneous DNA-GMP fibrillar network was observed, with an enhancement in the relative green fluorescence intensity and dominated over the weak blue fluorescence of DNA, leading to the exclusive observation of green emission in the confocal laser microscopy images. Thus, from the controlled fluorescence microscopic studies of the DNA-GMP condensation, it could be inferred that the GMP concentration played a significant role in the π-π stacking pattern, thus resulting in a homogeneous fibrillar network at optimum GMP concentration.

In order to further ascertain the dynamic reconfiguration of the biocondensate, temperature-dependent studies were performed. The variable-temperature CD spectra of the DNA-GMP condensate (40 μg/mL DNA and 150 μM GMP) showed only a marginal change in the intensity of

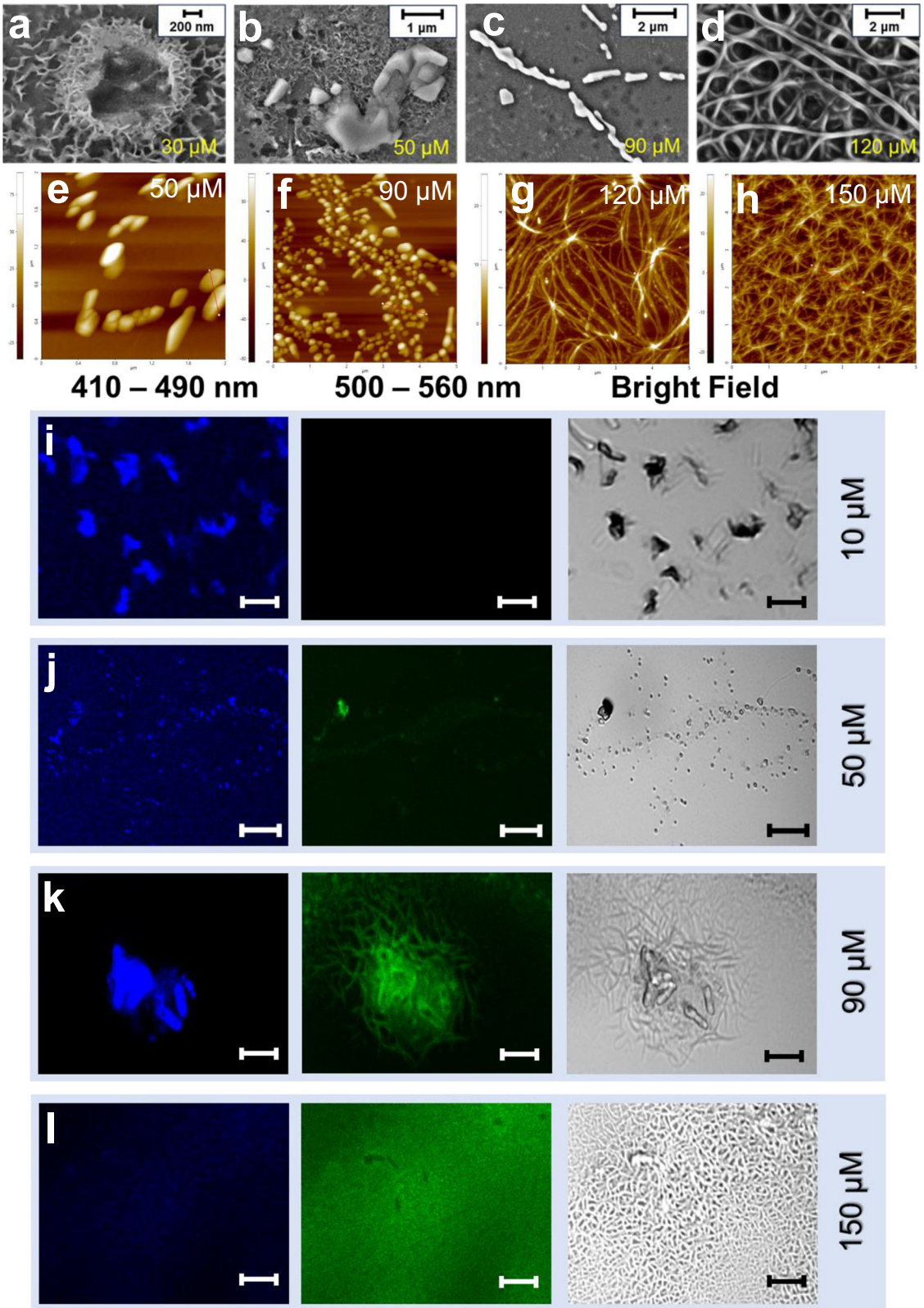

Fig. 3 | Kinetic morphological organization of DNA-GMP condensation. a–d Anisotropic morphological evolution of the DNA-GMP condensation with variable GMP concentration studied by FE-SEM images. **e–h** AFM images of morphological kinetic evolution. **i–l** Confocal fluorescence images of the evolution of green fluorescence with the increase in GMP concentration (scale bar: 5 μm).

the negative Cotton band at 250 nm, maintaining similar ellipticity across the temperature range of 10 °C to 50 °C (Supplementary Fig. 13A). On the other hand, the emission of ThT bound condensate was significantly quenched when temperature was increased from 10 °C to 50 °C (Supplementary Fig. 13B). At higher temperature, the ThT molecules which were bound in the rigid and more planar G4 grooves were released, thereby activating the nonradiative torsional relaxation channel[38]. The results showed the possibility of modulation in dynamics of π-π interactions within the condensate at variable temperature. This was verified from the FESEM studies (Supplementary Fig. 14), which showed that the highly fibrillar and entangled condensate network at 30 °C, was converted into small nanoaggregates at 40 °C. At 50 °C, one exclusively finds aggregated microspheres decorated with the smaller aggregates with the protrusion of thin petal-like structures from the surface, which were formed at the expense of the nanofibrils. Further fractal self-assembly of these microstructures led to complex flower-like superstructures at 60 °C. This morphological evolution might be attributed to the dynamic liquid condensation phases of DNAs, which forms noncanonical linear aggregates through physical aggregation. As the temperature increases, the weakening of end-to-end adhesion in DNA-wrapped G4-condensation leads to the formation of smaller linear aggregates on the surface of the homogeneous fibrillar network[40]. The progression in the self-assembly of these linear aggregates along a uniaxial columnar pathway, eventually creates petal-like structures on the surface, which gradually evolve into a flower-like spherical morphology in the matrices[41,42]. Notably, the temperature dependent morphological rearrangements were dynamic and reversible in nature as the DNA-GMP bio-condensates spontaneously reassemble and recovered to their highly fibrillary morphology upon cooling down to 30 °C (Supplementary Fig. 15).

DNA/GMP extensive condensation leading to hydrogelation

As the bio-condensation of DNA and GMP lead to fibrillar nanostructures in dilute condition, we further studied their self-assembly process at higher concentration of both the constituents. When the condensation was carried out at a concentration of 40 mg/mL of salmon milt DNA and 150 mM of GMP, a highly stable light-yellow hydrogel was formed spontaneously (Fig. 4a). Controlled experiments suggest that the gelation can take place in a wide range of concentration with minimum of 30 mg/mL of DNA and 75 mM of GMP respectively (Supplementary Fig. 16). The hydrogel formed is stable within the pH range of 1.5-11 (Supplementary Fig. 17) and the hydrogel can be molded into various shapes using different templates (Supplementary Fig. 18A). Thin membranes of the hydrogel also can be obtained by slicing or thin coating followed by drying even at room temperature (Supplementary Fig. 18B). FESEM image of the diluted hydrogel shows the dense entangled fibres (Supplementary Fig. 19A). The fibrillar morphology of the diluted hydrogel was also observed in the HRTEM images (Supplementary Fig. 19B), suggesting that the condensate and hydrogel share similar morphological patterns.

The powder X-ray diffraction pattern of the lyophilized DNA-GMP hydrogel showed a diffraction peak at 2θ of 2.4° ($d = 3.85$ nm) and 2θ of 27.8° ($d = 0.32$ nm) corresponding to the diameter of a single G-tetrad and interplanar separation of G-tetrads through π- π stacking respectively[43] (Supplementary Fig. 20). In the FT-IR spectra, the bands at 1218 cm^{-1} and 1067 cm^{-1} in GMP, corresponding to the $P = O$ and P−O stretching bands of the phosphate groups, were significantly reduced in intensity in the DNA-GMP hydrogel suggesting the involvement of phosphate groups in extensive hydrogen bonding. Furthermore, the bands at 1687 cm^{-1} (C=O stretching) and 1600 cm^{-1} (N-H bending) in GMP were shifted to 1700 cm^{-1} and 1606 cm^{-1} respectively, suggesting the involvement of these functional groups of GMP in G-quadruplex formation[44,45] (Supplementary Fig. 21). These studies confirmed that at higher concentration also similar mechanism follows, where, randomly coiled biomass DNA form ordered helical strands by wrapping around the π-π stacked G4 nano-strands, which entangle densely to form a porous network of hydrogel with absorbed water.

Next, the possibility of DNA-GMP hydrogel formation in an organic-aqueous solvent mixture was explored. Using the same concentrations of DNA and GMP (40 mg mL^{-1} and 150 mM respectively) as used for hydrogel formation, we observed stable organogel formation in 20% v/v (ODG20), 40% v/v (ODG40), and 60% v/v (ODG60) of glycerol-water mixture as a solvent. The transparent light yellow-colored gels were mechanically rigid with a shear stress of 10.8 kPa (Supplementary Fig. 22). In other solvent mixtures, such as DMSO-water, acetonitrile-water, or ethanol-water, only precipitates were formed. This can be attributed to the insolubility of GMP in common organic solvents. The ODG60 gel did not get frozen even after keeping it at −20 °C for 20 days, which can be attributed to the anti-freezing properties of glycerol. This was further quantitatively studied in a systematic dehydration process, where only 10% weight loss was observed in the ODG60 gel even after keeping for 7 days at −20 °C (Supplementary Fig. 23). The DNA-GMP gels formed in a biocompatible solvent such as glycerol with excellent mechanical and anti-freezing properties can be useful for biomedical and tissue engineering applications, even under extreme conditions[46].

The mechanical and viscoelastic properties of the prepared DNA-GMP hydrogel were evaluated via oscillatory rheological measurements. In the dynamic strain and frequency sweep studies, the storage modulus (G′) of the hydrogel was found to be several orders higher than the loss modulus (G″), indicating dominance of the elastic behavior over its viscous nature (Fig. 4b, c). Dynamic strain sweep measurements demonstrate the effect of GMP concentration (low, medium and high) on the mechanical properties of the DNA-GMP hydrogel. The storage modulus (G′) increases up to a GMP concentration of 150 mM, but decreases with further increases in concentration (Supplementary Fig. 24). Therefore, the optimal GMP concentration for the DNA-GMP hydrogel, providing the best mechanical properties, is 150 mM. Further, much higher storage modulus (G′) of DNA-GMP gels with increasing amount of glycerol suggests its role in enhancing the mechanical robustness (Supplementary Fig. 25). The physical integrity of the hydrogel was further assessed through a thixotropic loop test. At a low strain of 1%, the hydrogel shows elastic nature (G′>G″), whereas, the viscous nature dominates upon increasing the strain to 500% (G″>G′). The hydrogel was reverted back immediately to its original elastic state when the strain was reduced to 1% and this behavior can be observed over several cycles (Fig. 4d). This shows excellent injectability capabilities of the hydrogel (Supplementary Fig. 26). In addition, the self-healing properties of the DNA-GMP hydrogels were studied by adjoining the surfaces of two dye-doped pieces, where a robust and healed hydrogel was obtained within 5 min, without any external energy input (Fig. 4e). The stiffness and toughness of the healed hydrogel suggest that due to the involvement of non-specific supramolecular interactions such as H- bonding and π-π stacking, a quick recovery and fluidity of the hydrogel could be achieved (Supplementary Fig. 27).

The DNA-GMP hydrogel was converted into a sol upon heating at 50 °C, which could be reverted back to a gel upon cooling to 25 °C. This thermo-reversible behavior could be observed over several cycles without any appreciable changes in their mechanical robustness (Fig. 4f, g). The gel-to-sol transition, driven by temperature, can be linked to the dynamic reconfigurability of the DNA-GMP condensate, suggesting that dynamic morphological changes significantly impact the self-assembly process. Further, a pH-responsive reversible sol-gel transition was observed in the DNA-GMP hydrogel. When the pH was increased to 12, the hydrogel was converted into a sol, which could be reverted back upon bringing the pH back to 5.5. This pH tuneable gel-sol transition could also be repeated over several cycles (Fig. 4h). In a highly basic medium, the hydrogen-bonded G-quadruplex network is disrupted leading to a sol, which can be reformed under suitable acidic environment. As the fibril network was knitted through only weak interactions, the gel to sol transition can be easily altered by external stimuli like temperature and pH. Due to the temperature-responsive nature of the hydrogel, a strain sweep experiment was conducted to confirm its stability at physiological pH and 37 °C (Supplementary Fig. 28). The storage and loss moduli remained unaffected at this

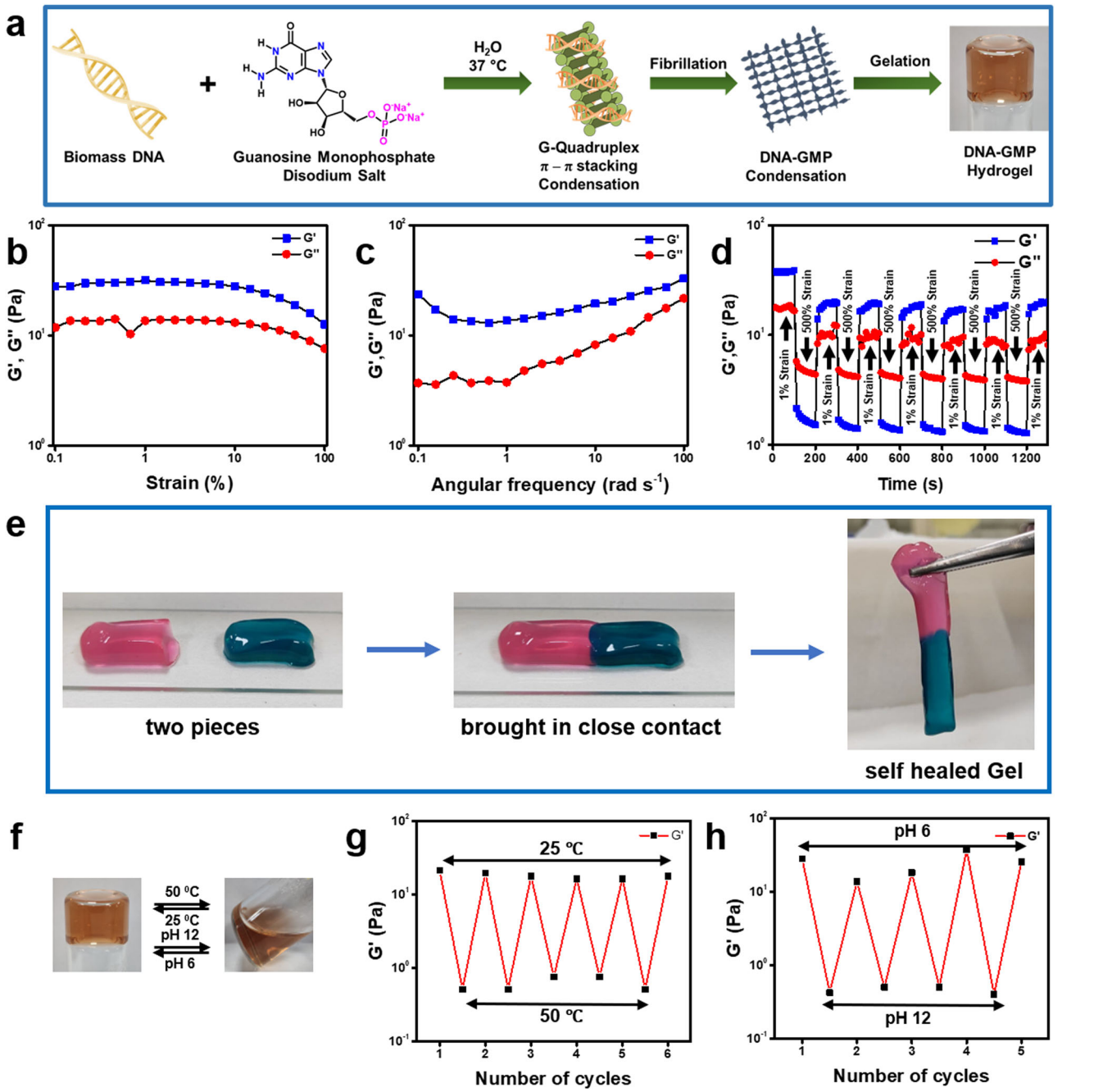

Fig. 4 | Synthesis and mechanical property investigations of the DNA-GMP hydrogel. a Transformation of DNA-GMP condensate to DNA-GMP hydrogel at higher concentration. **b** Dynamic strain−sweep rheological experiment of DNA-GMP hydrogel, (**c**) angular frequency sweep experiment for the hydrogel at constant strain of 1%, (**d**) Thixotropic loop measurement for DNA-GMP hydrogel at a constant angular frequency of 10 rad s^{-1} with changing the strain from 1% to 500%, (**e**) Self-healing ability of the DNA-GMP hydrogel upon close contact, (**f**) Stimuli responsiveness of the DNA-GMP hydrogel upon temperature of pH, (**g**) Cyclic thermo-reversible rheological study of the hydrogel and (**h**). Cyclic pH-reversible rheological study of DNA-GMP hydrogel.

temperature, indicating the hydrogel's favorable mechanical integrity for various biological applications.

As the constituents of the hydrogel are all nucleic acids, it is expected that the hydrogel will show high biocompatibility. This was reflected in the IC_{50} values of GMP, DNA and DNA-GMP hydrogel which was 760 μM, 1814 μM, and 1496 μM respectively using AGS cells. Further, cell death studies assessed by IC_{10} values showed that the DNA-GMP gel imparted no toxicity on both AGS and A549 cells. DNA-GMP showed a significantly lesser apoptotic cells in both A549 ($p < 0.05$) and AGS ($p < 0.001$) cells in comparison to untreated cells, showing its biocompatible nature[47] (Supplementary Fig. 29, 30).

DNA/GMP condensate hydrogel as a dense phase hydrotropic drug carrier

Supramolecular hydrogels derived from biomolecules hold potential as a drug carrier. Especially a noncanonical nucleic acid conformation such as G-quadruplex is found to be overrepresented in cancer containing genes and has been used as a valuable tool in cancer therapeutics[48–51]. Although both DNA and GMP are highly water soluble, the G-quadruplex can act as a hydrotropic system by trapping water insoluble molecules in the small cavities formed by vertically stacked guanine tetrads[52–54] (Fig. 5a). Also, the dynamic reconfigurability and the excellent stimuli responsiveness of the hydrogel (Fig. 4) provides alteration towards from fibrillar morphology to

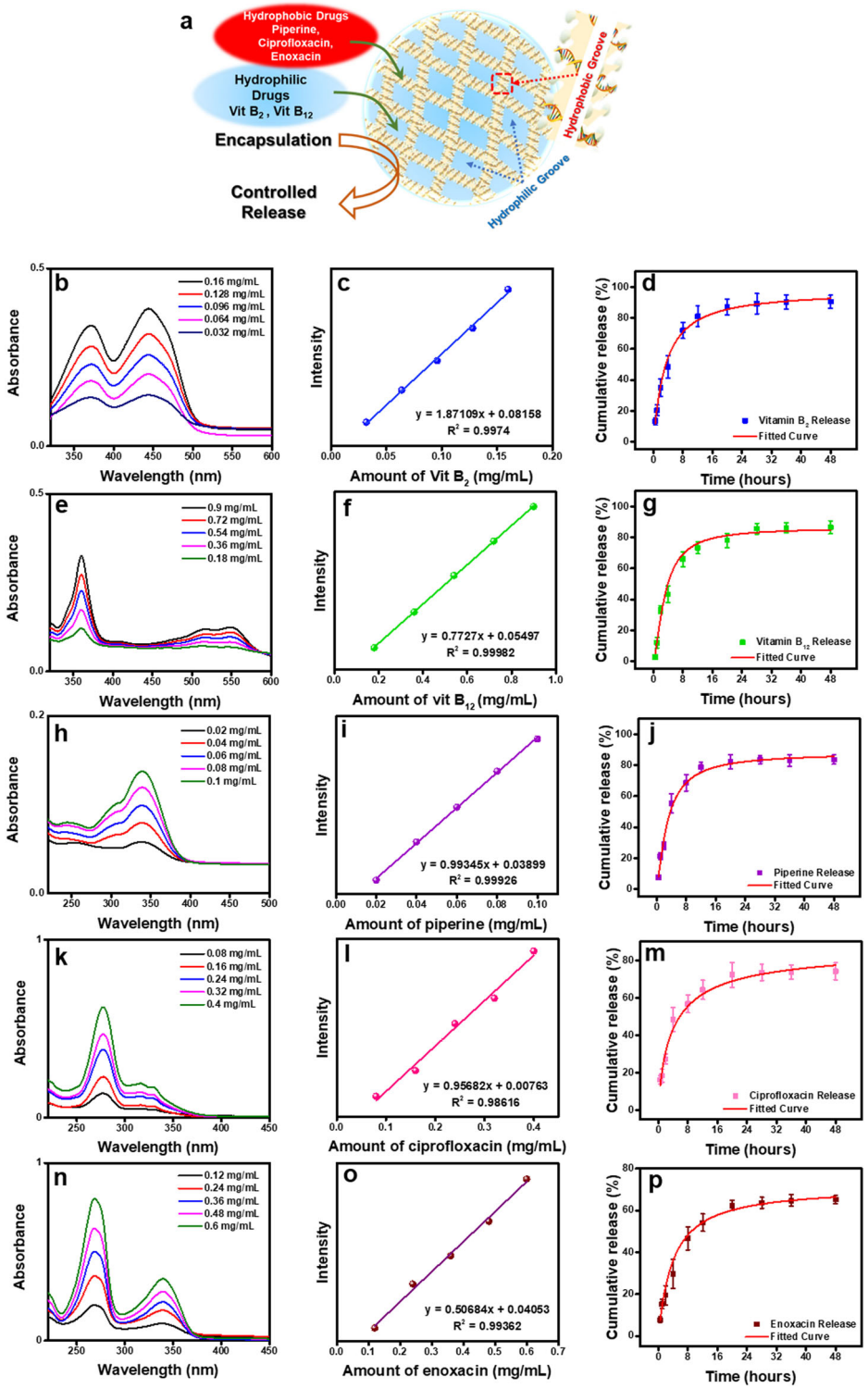

Fig. 5 | DNA-GMP hydrogel as a hydrotropic drug carrier. a Diagram illustrating the site-specific encapsulation of hydrophobic and hydrophilic drugs within the DNA-GMP hydrogel fibers. UV-vis spectra of (**b**) vitamin B_2, (**e**) vitamin B_{12}, (**h**) piperine, (**k**) ciprofloxacin, and (**n**) enoxacin in simulated body fluid (pH 7.4, phosphate buffer saline solution) at different concentrations. Calibration curves of (**c**) vitamin B_2, (**f**) vitamin B_{12}, (**i**) piperine, (**l**) ciprofloxacin, and (**o**) enoxacin. Release profiles of (**d**) vitamin B_2, (**g**) vitamin B_{12}, (**j**) piperine, (**m**) ciprofloxacin, and (**p**) enoxacin, from drug-loaded DNA-GMP hydrogel and corresponding polynomial fitting curves.

petal condensed microspheres (Supplementary Fig. 15) which facilitates the ease for encapsulation and sustained release of drug molecules at physiological conditions. Therefore, we focused on using the DNA-GMP hydrogel as a drug carrying agent for both water-soluble and sparingly water-soluble drugs (Supplementary Fig. 31). We have studied two vitamins: (a) Vitamin B_2, riboflavin[55] and (b) Vitamin B_{12}, cyanocobalamin[56] as model water soluble drugs to be entrapped in the DNA-GMP hydrogel. Addition of vitamins, DNA and GMP in an aqueous medium, under physiological conditions resulted in the vitamin encapsulated hydrogels and after repeated washing, it was found that the hydrogel could encapsulate 86% and 78% of vitamin B_2 and B_{12} (Supplementary Figs. 32 and 33).

In order to establish the DNA-GMP hydrogel as a carrier for hydrophobic drugs, the loading of alkaloid drug molecule Piperine (with antimicrobial, antidepressant, anti-inflammatory, and anti-angiogenic and potential anti-cancer properties)[57], fluoroquinolone-based drug Ciprofloxacin (used for the treatment of bone and joint infections, intra-abdominal infections)[58,59] and Enoxacin (antibacterial agent used in the treatment of urinary tract infections and gonorrhea)[60,61] were studied.

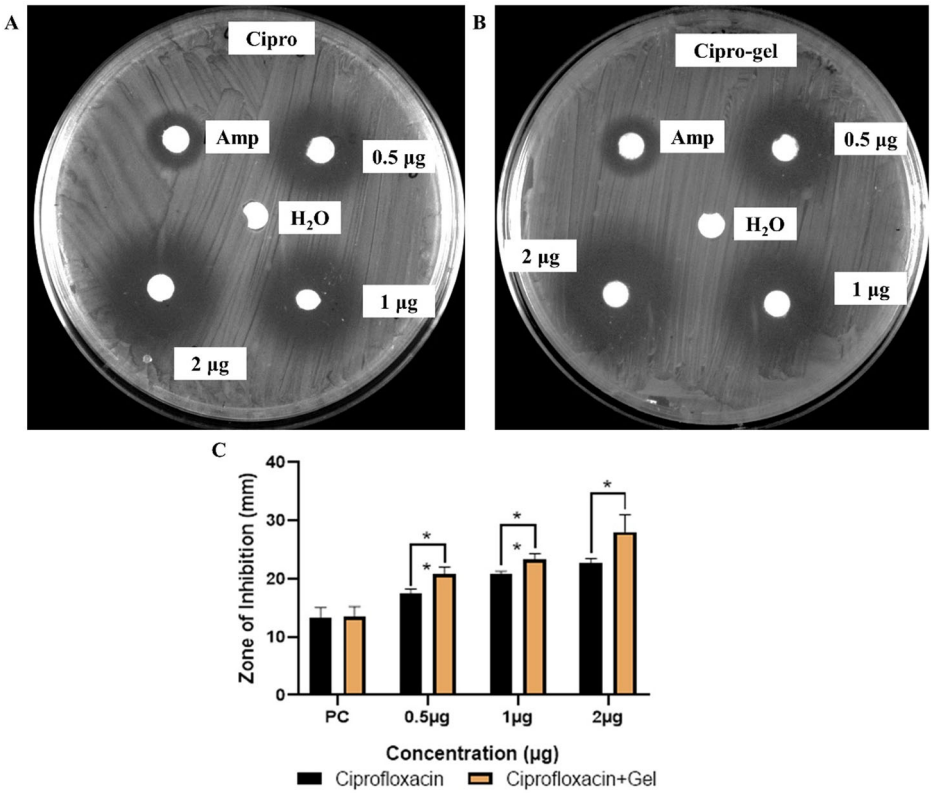

Fig. 6 | Anti-bacterial activity of gel compound against *E. coli*. **A** Representative clear zone of inhibition of Ciprofloxacin against *E. coli*, (**B**) Representative clear zone of inhibition of Ciprofloxacin-gel against *E. coli* and (**C**) Bar graph showing the antibacterial activity of the Cipro and Cipro-gel compound against *E. coli*. Cipro-gel possesses the significantly more anti-bacterial activity than positive control Ampicillin and other compound ciprofloxacin. The experiment was performed for two biological replicates, and the results are shown as the mean ± SD for two independent experiments. Data were statistically analyzed using an unpaired *t*-test. *p* values were estimated using GraphPad Prism version 8, and *p* values of 0.05, 0.01, and 0.001 were considered statistically significant and represented by */#, **/##, and ***/###, denoting upregulation/downregulation respectively.

Mixing of the drug molecules, DNA and GMP in an aqueous medium and heating at 37 °C led to the drug-loaded hydrogels. Although all these drug molecules were only sparingly soluble in water, however, they could be easily mixed in an aqueous medium containing DNA and GMP. After several washing cycles of the drug-loaded hydrogel using PBS buffer, the encapsulation efficiency was estimated by UV-visible spectroscopy using calibration curves and was found to be 95%, 92% and 77% for Piperine, Ciproflaxacin and Enoxacin respectively (Supplementary Figs. 34–36). This in situ drug loading process in the hydrogel was highly efficient for different drug molecules and unbound drug molecules could be removed easily to avoid any side effects. The maximum drug loading capacity per 1 mL of hydrogel was 1.8 mg for piperine, 2.4 mg for ciprofloxacin, and 2.1 mg for enoxacin.

In a typical drug release experiment, all the drug-loaded hydrogels (1 mL) were separately covered with PBS buffer solution (3 mL, pH 7.4) and incubated at 37 °C. To determine the release at a regular time interval, an aliquot of 400 µL was collected and replaced with fresh buffer. Drug release profiles were monitored by UV-visible spectrophotometry (Supplementary Fig. 37) at the absorption maxima of the respective drugs with the help of calibration curves (Fig. 5b, c, e, f, h, i, k, l, n, o). The DNA-GMP hydrogel showed a sustained release of 81% and 91% of vitamin B_2 after 12 and 48 h respectively (Fig. 5d). On the other hand, a more sustained release of 73% after 12 h and 87% after 48 h were observed in case of much bulkier vitamin B_{12} (Fig. 5g). In case of the hydrophobic therapeutic drug piperine, a sustained delivery was achieved with a release rate of 78.9% at 12 h and 83.7% after 48 h with DNA-GMP hydrogel (Fig. 5j). Due to potential anti-cancer property of piperine, the release profile was further studied at pH 4.4 and a higher rate of release was observed after 12 (86.8%) and 36 h (95.8%), showing much higher drug release under pH conditions relevant to cancerous environments (Supplementary Fig. 38). Ciprofloxacin shows a sustained release profile of 64.3% at 12 h and 74.2% after 48 h, respectively (Fig. 5m). Again, for the antibacterial drug enoxacin, a sustained release of 54% and 65% were obtained at 12 h and 48 h respectively (Fig. 5p). A time-dependent drug release experiment was conducted to elucidate the drug delivery mechanism (Supplementary Fig. 39). The results indicated a first-order, diffusion-based release, where the swelling of the fibrillar network enables the entrapped drug to diffuse into the buffer medium. Both hydrophilic and hydrophobic drugs exhibited similar sustained release profiles, suggesting that the hydrogel follows a consistent release mechanism for all drug types (Supplementary Fig. 40). The stability of the drug-loaded hydrogel and the impact of drug molecules on the bio-condensation process were evaluated. SEM images showed no significant changes in the hydrogel morphology after drug loading (Supplementary Fig. 41A). The mechanical properties of the drug-loaded hydrogels also remained comparable to those of the DNA-GMP hydrogel (Supplementary Fig. 41B). Additionally, the shelf-life and anti-leakage properties were tested, revealing that the hydrogel effectively encapsulated the drugs for up to 28 days, with minimal drug leakage observed during each weekly wash (Supplementary Fig. 42). Therefore, the hydrogel serves as an efficient carrier for both water-soluble and sparingly soluble drugs via a diffusion mechanism, offering advantages over previous reports (Supplementary Table 2) and providing new impetus for sustained drug delivery.

The hydrogel enhances the antibacterial activity of the encapsulated drug

To demonstrate the drug-carrier capacity of the DNA-GMP hydrogel in real-time biological system, we conducted a systematic antibacterial assay using ciprofloxacin as a model drug. The antibacterial efficacy of ciprofloxacin (Cipro) and ciprofloxacin-loaded DNA-GMP hydrogel (Cipro-gel) was tested against *E. coli* using a disc diffusion assay. Clear inhibition zones around the disks indicated that both formulations effectively inhibited bacterial growth. For pristine ciprofloxacin, the zone of inhibition increased with higher concentrations, with 0.5 µg showing a larger zone than the positive control, ampicillin. Similarly, for Cipro-gel, increasing the drug concentration enhanced the inhibition zone, with 0.5 µg showing greater inhibition than both the positive control ampicillin and ciprofloxacin alone (Fig. 6). These results suggest that encapsulating the drug in the DNA condensate hydrogel enhances its antibacterial efficacy, demonstrating that the DNA-GMP hydrogel serves as an excellent drug carrier with improved biological activity.

Nanoparticle/Quantum Dot embedded smart hydride biomolecular hydrogelation

Finally, we explored the possibility of using DNA-GMP hydrogel for trapping water-soluble nanoparticles (NPs) resulting in hybrid hydrogels. Citrate-stabilized Au NPs, Mercaptosuccinic acid capped Cadmium Telluride (CdTe) quantum dots and magnetic Fe_3O_4 NPs could be easily loaded in the hydrogel matrix by simply mixing DNA and GMP to an aqueous nanoparticle solution at 37 °C. Au NP loaded hydrogels showed a slightly red-shifted and broadened peak, which may be attributed to the slight aggregation of Au NPs owing to the acidity of DNA strands[62,63] (Supplementary Fig. 43). In the case of CdTe embedded hydrogel, a red-shift of 9 nm in the emission maxima was observed, which can be attributed to the energy transfer between the QDs in the closely spaced hydrogel matrix[64,65] (Supplementary Fig. 44). The Fe_3O_4 NP loaded hydrogels showed magnetic activity and attracted by an external magnetic field (Supplementary Movie 1). The results suggest that the DNA-GMP hydrogel matrix can be used as a platform for development of "smart" hybrid hydrogels.

Conclusion

In conclusion, taking a cue from DNA condensation in chromatin, we have demonstrated a facile pathway for biomass DNA condensation through a simple mixing of DNA with a nucleotide guanosine monophosphate. The bio-condensate was formed through a synergistic effect, where the acidic nature of DNA induced the formation of G4 supramolecular structures. The randomly coiled DNA macromolecules wrapped around the stacked G4 strands resulting in a helical fibrillar network. The spectroscopy and microscopy studies showed the concentration-dependent self-assembled process leading to highly entangled network. At higher concentration of the nucleic acid constituents, a mechanically robust, stimuli-responsive, and self-healable hydrogel could be obtained. The process can be extended to form an organogel, membranes, and composite hydrogels. Given the abundance of biomass DNA, this versatile, programmable, and biocompatible "all-nucleic" DNA-GMP hydrogel could serve as a sustainable alternative to petroleum-based polymers in the production of soft materials. The DNA-GMP hydrogel can function as a universal hydrotropic drug carrier, promoting a steady release of both hydrophobic and hydrophilic drugs. The bio-condensate and hydrogel formation using biomass DNA in the presence of GMP through non-covalent interactions paves away a simple methodology for soft material fabrication with application potential for advanced applications such as DNA switches and DNA-based machines. Using a similar protocol, the bio-condensation process can be extended to RNA, which we are currently pursuing.

Methods

Synthesis and characterization of biomass DNA-GMP condensates

Mixing salmon milt DNA (40 μg/mL) with 150 μM of disodium guanosine monophosphate ($GMPNa_2$) in water yields a homogeneous, transparent solution. After incubating this solution at 30 °C for 12 h, the formation of condensate is observed visually by using a simple red laser, which demonstrates a visible Tyndall effect. For further controlled experiments, condensates were prepared using the same protocol but with varying concentrations of GMP. These different GMP concentration condensates were then subjected to circular dichroism (CD) spectroscopy and field emission scanning electron microscopy (FE-SEM) imaging. For variable temperature studies, the condensate formed with 40 μg/mL DNA and 150 μM GMP was used. For steady-state fluorescence (FL) measurements, DNA-GMP condensates were prepared with varying concentrations of GMP, and all samples were incubated with 10 μM Thioflavin T (ThT) dye. The ThT-labeled condensates were excited at 425 nm for steady-state FL measurements. For confocal imaging, the same ThT-labeled condensates, prepared with different GMP concentrations, were drop-cast onto glass cover slips, and confocal microscopy was performed using a laser with an excitation wavelength of 405 nm. The zeta potential of the condensates was measured at various stoichiometric ratios, maintaining constant concentrations of DNA and GMP during condensation.

Synthesis of biomass DNA hydrogel

For the synthesis of the DNA-GMP hydrogel, 40 mg of salmon test DNA was precisely dissolved in 1 mL of Mili-Q water, with gentle stirring and maintaining a constant heat of 37 °C resulting in a homogeneous solution. Following 5 min of stirring, 61.2 mg (150 mM) of Guanosine Monophosphate Disodium Salt was added to the solution. The solution promptly transformed into a transparent, light brown color. Within 2–3 min of cooling to room temperature, a transparent DNA-GMP hydrogel was obtained. The confirmation of hydrogel formation was obtained through the simple inverse tube method. For the synthesis of organogel, salmon Tests DNA was used with the same synthetic strategy. Instead of water, a mixture of glycerol and water at different ratios, 20% (v/v), 40% (v/v), and 60% (v/v) glycerol/water mixture were used for the preparation of organogels ODGH-20, ODGH-40 and ODGH-60 respectively. All the organogels were prepared at mild heating at 37 °C and gels were stable and can be prepared in various molds of diverse shapes.

Mechanical properties studies

The rheological investigations of synthesized hydrogels were performed using a parallel plate geometry of diameter 25 mm. The dynamic strain sweep measurements were taken at a constant angular frequency (ω) of 10 $rads^{-1}$ and frequency sweep experiments of hydrogel was measured at a constant strain (γ) value = 1% at 25 °C. The thixotropic step-strain measurements with respect to time intervals were carried out at variable strain values of 0.1% and 500% at a constant 10 $rads^{-1}$ of ω^1.

Two different dye-loaded gels each of 2 mL synthesized inside rectangular molds. After aging, both dye-loaded hydrogels were taken close to each other joined using mild mechanical press and after 5 min the self-healed hydrogel could be lifted in air. The storage modulus (Ǵ) values of the original and self-healed gel were calculated at 1% constant strain. The dynamic sweep test followed by time-dependent storage and loss modulus calculation at a constant strain at 1% was also evaluated to confirm the self-healing ability[2].

To obtain the thermo-reversibility property of the hydrogel, the gel was heated homogeneously at 50 °C to form a solution and evaluated the mechanical strength. The same gel was cooled down to room temperature for reversible formation of gel and evaluated the mechanical properties. To study the effect of the pH-reversibility, 5 μL of 4 M NaOH solution was added that increases the pH of the medium to 12. The hydrogel was completely dissociated to sol state within 5 min. The sol was converted into a gel upon addition of 5 μL of 4 M H_2SO_4 (pH 5.5) and this reversible sol-gel transition could be obtained for 4 cycles.

In vitro biocompatibility test

Mammalian cell culture. A549 (human lung adenocarcinoma) and AGS (human gastric adenocarcinoma) cells were cultured in Dulbecco's minimal essential medium (DMEM) supplemented with 10% fetal bovine serum (FBS) and 1% antibiotic and antimycotic solution. Cells were cultured at 37 °C in a humidified incubator at 5% CO_2. Compounds for treatment were prepared in DMEM supplemented with 10% FBS.

Cell viability assay

For the MTT assay, about 10,000 cells per well were seeded in 96-well plates and incubated for 24 h. Further, cells were treated with different concentrations of GMP, DNA, and DNA-GMP for 24 h. Subsequently, media was extracted from the wells, and 50 μL per well of MTT dye (0.5 mg/mL in PBS) was added and incubated for 3 h at 37 °C. Next, 100 μL of DMSO was added to each well, and absorbance at 570 nm was recorded using a microplate reader.

EB-AO staining

The assessment of the apoptotic, necrotic, and live cells after exposure to compounds was done by EB/AO dual staining. The cells were stained with acridine orange and ethidium bromide mixture (100 µg/ml each) for 20 min at 37 °C followed by PBS washing by PBS. The analysis of the cell stage (apoptotic/ necrotic) was done manually by observing the color characteristics.

Statistical analysis

All the experimental results were recorded from a set of triplicates. Data were statistically tested using an unpaired t-test. p values were estimated using GraphPad Prism version 8, and p values of 0.05, 0.01, and 0.001 were considered statistically significant and represented by */#, **/##, and ***/###, respectively.

Drug loading and encapsulation efficiency

A 1 mg mL^{-1} aqueous solution comprising Riboflavin (vitamin B_2), Cobalamin (vitamin B_{12}), piperine, ciprofloxacin, and enoxacin was prepared through continuous stirring. To this solution containing the drug molecules, biomass DNA was added, followed by the gradual addition of GMP-Na_2 at the same concentration (40 mg mL^{-1} for DNA and 150 mM for GMP), while maintaining a constant temperature of 37 °C. After a cooling and aging period of 10 min, self-standing stable drug-loaded hydrogels were successfully formed. These hydrogels were subsequently employed for investigating the encapsulation and sustained drug release behavior of the hydrogel. 1 mg mL^{-1} of drug-dissolved solution was used for the preparation of the hydrogel. To remove the unbound drug molecules, the hydrogel was washed with 3 mL of pH 7.4 PBS solution. The absorbance of washed supernatant was measured using a UV-vis spectrophotometer. The amount of vitamin or drug molecules encapsulated inside the hydrogel matrix was estimated by subtracting the vitamin or drug present in the supernatant buffer from the amount taken initially, and the loading percentage was calculated using the following equation:

$$\text{Encapsulation efficiency}\,(\%) = \frac{\text{Amount of Vit/Drug present after washing}}{\text{Initial amount of Vit/Drug}} \times 100$$

To study the sustained release profile of vitamin and piperine-loaded hydrogels, 1 mL of vitamin and piperine-loaded hydrogels were taken in three separate glass vials, and 3 mL of phosphate buffer saline solution (10 mM PBS, pH 7.4) was added. All three vials were incubated at 37 °C. At different time intervals, a small aliquot of 400 µL was removed and collected separately from each vial and fresh PBS solution of same amount of 400 µL was added to each vial. The absorbance of collected samples was measured at the wavelength of 445 nm, 550 nm, 340 nm, 320 nm, and 339 nm for vitamin B_2, vitamin B_{12}, piperine, ciprofloxacin, and enoxacin, respectively, using a UV-vis spectrophotometer. To ascertain the accuracy, the experiments were performed three times and the average value with an error bar was plotted to the sustained drug release profile. The calculation for the cumulative release of the drug is shown below,

$$\text{The cumulative release of drug} = \frac{M_t}{M_\infty} \times 100$$

Where M_t and M_∞ are the amount of drug released at time t and the initial quantity of drug encapsulated inside the hydrogel, respectively. From the calibration curve of each vitamin and drug, we got a linear relation between the concentration (amount) and absorbance value. Therefore, for the simplicity of calculation, we have taken the absorbance value directly to calculate the cumulative release of the drug.

To evaluate the shelf-life and anti-leakage properties of the drug-loaded hydrogel, samples were stored at 4 °C. At fixed intervals over a 7-day period, the hydrogels were washed with PBS buffer, and drug leakage was monitored by measuring the UV-visible absorbance of the supernatant.

Antibacterial activity

Bacterial strain. A gram-negative bacterial strain was used to check for antibacterial activity of the compounds. *Escherichia coli* (DH5α) was used in this study. *E. coli* was cultured in Luria Broth agar (Becton, Dickinson and Company, New Jersey, USA) and incubated at 37 °C for 12 h. Pure colonies were picked up and cultured in Luria broth media (Becton, Dickinson and Company, New Jersey, USA) overnight in a rotary shake of 220 rpm at 37 °C.

Disc diffusion method

The antimicrobial activity of gel compounds against the gram-negative bacterial strain was monitored with the disk diffusion method[66,67]. The E. coli strain was spread on the LB agar plate. The Ciprofloxacin compound and Ciprofloxacin-loaded DNA-GMP hydrogel compound was dissolved in H_2O. The different compound concentration was used 0.5, 1, and 2 µg, 10 µl of each solution was impregnated into sterile, blank discs of 6 mm in diameter. H_2O was used as negative control. Ampicillin (Himedia, India) (100 µg/µl) were used as positive control in E. coli. The plate was incubated at 37 °C for 24 h in their respective conditions and the zone of inhibition was measured. Antimicrobial activity was determined by measuring the zone of inhibition diameter (mm) around the discs. The assay was performed twice.

Preparation of nanoparticle-embedded biomass DNA hydrogels

A red fluorescent biomass DNA-GMP hydrogel was formed by the simple addition of 1 mL of water-soluble red fluorescent CdTe nanoparticle-containing solution to 40 mg Salmon tests DNA and 61.2 mg of Guanosine monophosphate disodium salt upon mild heating/cooling. Similarly, the addition of an aqueous solution containing Au nanoparticles gives the Au nanoparticle-embedded biomass DNA hydrogel. Also, magnetic iron oxide nanoparticles can be embedded inside the DNA hydrogel matrix by adding 5 mg iron oxide nanoparticles in a similar amount of DNA and GMP-Na_2. All the nanoparticle-embedded hydrogels are as stable as the DNA-GMP hydrogel and they can be easily patterned inside a mold or can be used to form membranes.

Data availability

The authors declare that all data supporting the findings of this study are available within the article and its Supplementary Information and supplementary data files. Raw files of main manuscript Figs. 1c, d, 2, 4b–d, 4g, h, 5b–p, and 6e are provided in Supplementary Data 1. All the data are also available on reasonable request from the corresponding author.

Received: 11 June 2024; Accepted: 1 November 2024;
Published online: 12 November 2024

References

1. Netzer, A., Katzir, I., Baruch Leshem, A., Weitman, M. & Lampel, A. Emergent properties of melanin-inspired peptide/RNA condensates. *Proc. Natl Acad. Sci. USA* **120**, e2310569120 (2023).
2. Lampel, A. Biology-inspired supramolecular peptide systems. *Chem* **6**, 1222–1236 (2020).
3. Boisvert, F.-M., van Koningsbruggen, S., Navascués, J. & Lamond, A. I. The multifunctional nucleolus. *Nat. Rev. Mol. Cell Biol.* **8**, 574–585 (2007).
4. Brangwynne, C. P. Phase transitions and size scaling of membrane-less organelles. *J. Cell Biol.* **203**, 875–881 (2013).
5. Brangwynne, C. P. et al. Germline P granules are liquid droplets that localize by controlled dissolution/condensation. *Science* **324**, 1729–1732 (2009).
6. Fyodorov, D. V., Zhou, B.-R., Skoultchi, A. I. & Bai, Y. Emerging roles of linker histones in regulating chromatin structure and function. *Nat. Rev. Mol. Cell Biol.* **19**, 192–206 (2018).
7. Zhou, K., Gaullier, G. & Luger, K. Nucleosome structure and dynamics are coming of age. *Nat. Struct. Mol. Biol.* **26**, 3–13 (2019).

8. Kornberg, R. D. Chromatin structure: a repeating unit of histones and DNA. *Science* **184**, 868–871 (1974).
9. Kornberg, R. D. & Thomas, J. O. Chromatin structure: oligomers of the histones. *Science* **184**, 865–868 (1974).
10. Longstreet, A. R. & McQuade, D. T. Organic reaction systems: using microcapsules and microreactors to perform chemical synthesis. *Acc. Chem. Res.* **46**, 327–338 (2013).
11. Krinsky, N. et al. Synthetic cells synthesize therapeutic proteins inside tumors. *Adv. Healthc. Mater.* **7**, 1701163 (2018).
12. Veis, A. A review of the early development of the thermodynamics of the complex coacervation phase separation. *Adv. Colloid Interface Sci.* **167**, 2–11 (2011).
13. King, J. T. & Shakya, A. Phase separation of DNA: from past to present. *Biophys. J.* **120**, 1139–1149 (2021).
14. Landenmark, H. K. E., Forgan, D. H. & Cockell, C. S. An estimate of the total DNA in the biosphere. *PLoS Biol.* **13**, e1002168 (2015).
15. Bar-On, Y. M., Phillips, R. & Milo, R. The biomass distribution on Earth. *Proc. Natl Acad. Sci. USA* **115**, 6506–6511 (2018).
16. Lee, J. B. et al. A mechanical metamaterial made from a DNA hydrogel. *Nat. Nanotechnol.* **7**, 816–820 (2012).
17. Um, S. H. et al. Enzyme-catalysed assembly of DNA hydrogel. *Nat. Mater.* **5**, 797–801 (2006).
18. Meng, H.-M. et al. DNA dendrimer: an efficient nanocarrier of functional nucleic acids for intracellular molecular sensing. *ACS Nano* **8**, 6171–6181 (2014).
19. Lv, J., Dong, Y., Gu, Z. & Yang, D. Programmable DNA nanoflowers for biosensing, bioimaging, and therapeutics. *Chem. – A Eur. J.* **26**, 14512–14524 (2020).
20. Park, S. Y. et al. DNA-programmable nanoparticle crystallization. *Nature* **451**, 553–556 (2008).
21. Li, Z. et al. Making engineered 3D DNA crystals robust. *J. Am. Chem. Soc.* **141**, 15850–15855 (2019).
22. Hong, F., Zhang, F., Liu, Y. & Yan, H. DNA origami: scaffolds for creating higher order structures. *Chem. Rev.* **117**, 12584–12640 (2017).
23. Yue, L., Wang, S., Zhou, Z. & Willner, I. Nucleic acid based constitutional dynamic networks: from basic principles to applications. *J. Am. Chem. Soc.* **142**, 21577–21594 (2020).
24. Rhodes, D. & Lipps, H. J. G-quadruplexes and their regulatory roles in biology. *Nucleic Acids Res.* **43**, 8627–8637 (2015).
25. Wang, D. et al. Transformation of biomass DNA into biodegradable materials from gels to plastics for reducing petrochemical consumption. *J. Am. Chem. Soc.* **142**, 10114–10124 (2020).
26. Han, J., Guo, Y., Wang, H., Zhang, K. & Yang, D. Sustainable bioplastic made from biomass DNA and ionomers. *J. Am. Chem. Soc.* **143**, 19486–19497 (2021).
27. Nayak, S. et al. Biomass derived self-assembled DNA-dot hydrogels for enhanced bacterial annihilation. *Nanoscale* **14**, 16097–16109 (2022).
28. Shin, M. et al. DNA/tannic acid hybrid gel exhibiting biodegradability, extensibility, tissue adhesiveness, and hemostatic ability. *Adv. Funct. Mater.* **25**, 1270–1278 (2015).
29. Dong, J., O'Hagan, M. P. & Willner, I. Switchable and dynamic G-quadruplexes and their applications. *Chem. Soc. Rev.* **51**, 7631–7661 (2022).
30. Davis, J. T. G-quartets 40 years later: from 5′-GMP to molecular biology and supramolecular chemistry. *Angew. Chem. Int. Ed.* **43**, 668–698 (2004).
31. Chakraborty, A., Ravi, S. P., Shamiya, Y., Cui, C. & Paul, A. Harnessing the physicochemical properties of DNA as a multifunctional biomaterial for biomedical and other applications. *Chem. Soc. Rev.* **50**, 7779–7819 (2021).
32. Chantot, J. F., Sarocchi, M.-T. & Guschlbauer, W. Physico-chemical properties of nucleosides: 4. — Gel formation by guanosine and its analogues. *Biochimie* **53**, 347–354 (1971).
33. del Villar-Guerra, R., Trent, J. O. & Chaires, J. B. G-quadruplex secondary structure obtained from circular dichroism spectroscopy. *Angew. Chem. Int. Ed.* **57**, 7171–7175 (2018).
34. Chen, J. et al. Kinetic control of chirality and circularly polarized luminescence in G-quartet materials. *J. Mater. Chem. B* **9**, 7140–7144 (2021).
35. Adrian, M., Heddi, B. & Phan, A. T. NMR spectroscopy of G-quadruplexes. *Methods* **57**, 11–24 (2012).
36. Gao, M. et al. Temperature and pressure limits of guanosine monophosphate self-assemblies. *Sci. Rep.* **7**, 9864 (2017).
37. Renaud de la Faverie, A., Guédin, A., Bedrat, A., Yatsunyk, L. A. & Mergny, J.-L. Thioflavin T as a fluorescence light-up probe for G4 formation. *Nucleic Acids Res.* **42**, e65 (2014).
38. Mohanty, J. et al. Thioflavin T as an efficient inducer and selective fluorescent sensor for the human telomeric G-quadruplex DNA. *J. Am. Chem. Soc.* **135**, 367–376 (2013).
39. Bhasikuttan, A. C. & Mohanty, J. Targeting G-quadruplex structures with extrinsic fluorogenic dyes: promising fluorescence sensors. *Chem. Commun.* **51**, 7581–7597 (2015).
40. Zanchetta, G., Nakata, M., Buscaglia, M., Bellini, T. & Clark, N. A. Phase separation and liquid crystallization of complementary sequences in mixtures of nanoDNA oligomers. *Proc. Natl Acad. Sci. USA* **105**, 1111–1117 (2008).
41. Nakata, M. et al. End-to-end stacking and liquid crystal condensation of 6– to 20–base pair DNA duplexes. *Science* **318**, 1276–1279 (2007).
42. Zhu, G. et al. Noncanonical self-assembly of multifunctional DNA nanoflowers for biomedical applications. *J. Am. Chem. Soc.* **135**, 16438–16445 (2013).
43. Thakur, N., Chaudhary, A., Chakraborty, A., Kumar, R. & Sarma, T. K. Ion conductive phytic acid-G quadruplex hydrogel as electrolyte for flexible electrochromic device. *ChemNanoMat* **7**, 613–619 (2021).
44. Zuber, G., Prestrelski, S. J. & Benedek, K. Application of Fourier transform infrared spectroscopy to studies of aqueous protein solutions. *Anal. Biochem.* **207**, 150–156 (1992).
45. Gabelica, V. et al. Infrared signature of DNA G-quadruplexes in the gas phase. *J. Am. Chem. Soc.* **130**, 1810–1811 (2008).
46. Zhang, H. & Grinstaff, M. W. Recent advances in glycerol polymers: chemistry and biomedical applications. *Macromol. Rapid Commun.* **35**, 1906–1924 (2014).
47. Jakhmola, S. & Jha, H. C. Glial cell response to Epstein-Barr Virus infection: a plausible contribution to virus-associated inflammatory reactions in the brain. *Virology* **559**, 182–195 (2021).
48. Carvalho, J., Mergny, J.-L., Salgado, G. F., Queiroz, J. A. & Cruz, C. G-quadruplex, friend or foe: the role of the G-quartet in anticancer strategies. *Trends Mol. Med.* **26**, 848–861 (2020).
49. Kosiol, N., Juranek, S., Brossart, P., Heine, A. & Paeschke, K. G-quadruplexes: a promising target for cancer therapy. *Mol. Cancer* **20**, 40 (2021).
50. Bates, P. J. et al. G-quadruplex oligonucleotide AS1411 as a cancer-targeting agent: Uses and mechanisms. *Biochim. Biophys. Acta Gen. Subj.* **1861**, 1414–1428 (2017).
51. Li, K., Yatsunyk, L. & Neidle, S. Water spines and networks in G-quadruplex structures. *Nucleic Acids Res.* **49**, 519–528 (2021).
52. Li, J., Jin, X., Hu, L., Wang, J. & Su, Z. Identification of nonplanar small molecule for G-quadruplex grooves: Molecular docking and molecular dynamic study. *Bioorg. Med. Chem. Lett.* **21**, 6969–6972 (2011).
53. Xiao, F., Chen, Z., Wei, Z. & Tian, L. Hydrophobic interaction: a promising driving force for the biomedical applications of nucleic acids. *Adv. Sci.* **7**, 2001048 (2020).
54. Spiegel, J., Adhikari, S. & Balasubramanian, S. The structure and function of DNA G-quadruplexes. *Trends Chem.* **2**, 123–136 (2020).
55. Masschelin, P. M. et al. Vitamin B2 enables regulation of fasting glucose availability. *eLife* **12**, e84077 (2023).

56. Green, R. et al. Vitamin B12 deficiency. *Nat. Rev. Dis. Prim.* **3**, 1–20 (2017).
57. Tiwari, A., Mahadik, K. R. & Gabhe, S. Y. Piperine: a comprehensive review of methods of isolation, purification, and biological properties. *Med. Drug Discov.* **7**, 100027 (2020).
58. Mason, D. J., Power, E. G., Talsania, H., Phillips, I. & Gant, V. A. Antibacterial action of ciprofloxacin. *Antimicrob. Agents Chemother.* **39**, 2752–2758 (1995).
59. Vance-Bryan, K., Guay, D. R. P. & Rotschafer, J. C. Clinical pharmacokinetics of ciprofloxacin. *Clin. Pharmacokinet.* **19**, 434–461 (1990).
60. Henwood, J. M. & Monk, J. P. Enoxacin. *Drugs* **36**, 32–66 (1988).
61. Melo, S. et al. Small molecule enoxacin is a cancer-specific growth inhibitor that acts by enhancing TAR RNA-binding protein 2-mediated microRNA processing. *Proc. Natl Acad. Sci. USA* **108**, 4394–4399 (2011).
62. Taladriz-Blanco, P. et al. Reversible assembly of metal nanoparticles induced by penicillamine. Dynamic formation of SERS hot spots. *J. Mater. Chem.* **21**, 16880–16887 (2011).
63. Piao, J., Zhou, X. & Wu, X. Colorimetric human papillomavirus DNA assay based on the retardation of avidin-induced aggregation of gold nanoparticles. *Microchim. Acta* **185**, 537 (2018).
64. Franke, M. et al. Immobilization of pH-sensitive CdTe quantum dots in a poly(acrylate) hydrogel for microfluidic applications. *Nanoscale Res. Lett.* **12**, 314 (2017).
65. Zhou, Y. et al. Unusual multiscale mechanics of biomimetic nanoparticle hydrogels. *Nat. Commun.* **9**, 181 (2018).
66. Ngamsurach, P. & Praipipat, P. Antibacterial activities against Staphylococcus aureus and Escherichia coli of extracted Piper betle leaf materials by disc diffusion assay and batch experiments. *RSC Adv.* **12**, 26435–26454 (2022).
67. Razmavar, S., Abdulla, M. A., Ismail, S. B. & Hassandarvish, P. Antibacterial activity of leaf extracts of baeckea frutescens against methicillin-resistant Staphylococcus aureus. *Biomed. Res. Int.* **2014**, 521287 (2014).

Acknowledgements

The authors thank SIC, IIT Indore for instrumentation facilities, CRF, IIT Delhi for TEM facility. S.S. thanks Department of Chemistry, IISER Pune for pXRD facility. S.S. and N.V. thanks DST-Inspire for financial support. We also thanks Vaishali Saini for helping in performing antibacterial activity experiments. S.S. thanks Mr. Ravindra, Mr. Aditya. Mr. Tarun, Ms. Vidhi, and Ms. Amrita for their constant support.

Author contributions

S.S., N.T., and T.K.S. designed the project; S.S. conceived the project; N.D. and H.C.J. conducted the biological experiments; S.S. and T.K.S. wrote the manuscript with contributions from all authors.

Competing interests

The authors declare no competing interests.

Additional information

Supplementary information The online version contains supplementary material available at https://doi.org/10.1038/s42004-024-01353-6.

Correspondence and requests for materials should be addressed to Tridib K. Sarma.

Peer review information *Communications Chemistry* thanks Takanori Oyoshi, Arghya Paul, and Prolay Das for their contribution to the peer review of this work. Peer reviewer reports are available.